A RELM Earthquake Forecast Based on Pattern Informatics

James R. Holliday,[1,2] Chien-chih Chen,[3,2] Kristy F. Tiampo,[4] John B. Rundle,[2,1] Donald L. Turcotte,[5] and Andrea Donnellan[6]

INTRODUCTION

There have been a wide variety of approaches applied to forecasting earthquakes (Turcotte 1991; Kanamori 2003). These approaches can be divided into two general classes. The first is based on empirical observations of precursory changes. Examples include precursory seismic activity, precursory ground motions, and many others. The second approach is based on statistical patterns of seismicity. Neither approach has been able to provide reliable short-term forecasts (days to months) on a consistent basis.

Although short-term predictions are not available, longer-term seismic-hazard assessments can be made. A large fraction of all earthquakes occur in the vicinity of plate boundaries, although some do occur in plate interiors. It is also possible to assess the long-term probability of having an earthquake of a specified magnitude in a specified region. These assessments are primarily based on the hypothesis that future earthquakes will occur in regions where past, typically large, earthquakes have occurred (Kossobokov *et al.* 2000). As we will discuss, a more promising approach is to begin with the hypothesis that the rate of occurrence of small earthquakes in a region can be analyzed to assess the probability of occurrence of much larger earthquakes.

The Regional Earthquake Likelihood Models (RELM) forecast described in this paper is primarily based on the pattern informatics (PI) method (Rundle *et al.* 2002, 2003; Tiampo *et al.* 2002a, 2000c). This method identifies regions of strongly correlated fluctuations in seismic activity. These regions are the locations where subsequent large earthquakes have been shown to occur, therefore indicating a strong association with the high stress preceding the main shock. The fluctuations in seismicity rate revealed in a PI map may be related to the preparation process for large earthquakes. Seismic quiescence and seismic activation (Bowman *et al.* 1998; Wyss and Habermann 1988), which are revealed by the PI map, are examples of such preparation processes. The PI method identifies the existence of correlated regions of seismicity in observational data that precede the main shock by months and years. The fact that this correlated region locates the aftershocks as well as main shocks leads us to identify this region of correlated seismicity with the region of correlated high stress (Tiampo *et al.* 2002a, 2002b, 2002c).

The PI method does not predict earthquakes; rather it forecasts the regions (hot spots) where earthquakes are most likely to occur in the relatively near future (typically five to 10 years). The objective is to pinpoint more narrowly the areas of earthquake risk relative to those given by long-term hazard assessments. The result is a map of areas in a seismogenic region (hot spots) where earthquakes are likely to occur during a specified period in the future. In this paper a PI map is combined with historic seismicity data to produce a map of probabilities for future large events. These probabilities can be further converted, using Gutenberg-Richter scaling laws, to forecast rates of occurrence of future earthquakes in specific magnitude ranges. This forecast can be evaluated using the RELM likelihood test. In the following sections we present details of the PI method and the procedure for producing a composite forecast map. A discussion on binary forecasts and forecast verification techniques is provided in appendixes A and B.

THE PI METHOD

Our approach divides the seismogenic region to be studied into a grid of square boxes or pixels whose size is related to the magnitude of the earthquakes to be forecast. The rates of seismicity in each box are studied to quantify anomalous behavior. The basic idea is that any seismicity precursors represent changes, either a local increase or decrease of seismic activity, so our method identifies the locations in which these changes are most significant during a predefined change interval. The subsequent forecast interval is the five-year time window during which the forecast is valid. The box size is selected to be consistent with the correlation length associated with accelerated seismic activity (Bowman *et al.* 1998), and the minimum earthquake magnitude considered is the lower limit of sensitivity and completeness of the network in the region under consideration. The PI method as applied to California in this paper involves the following steps:

1. Department of Physics, University of California, Davis, USA
2. Computational Science and Engineering Center, University of California, Davis, USA
3. National Central University, Taiwan
4. Department of Earth Sciences, University of Western Ontario, Canada
5. Geology Department, University of California, Davis, USA
6. NASA Jet Propulsion Laboratory, USA

1. The seismically active region is binned into boxes of size 0.1° by 0.1° and all events having $M \geq 3.0$ are used. These boxes are labeled x_i. This is also the box size specified for the RELM forecast.
2. The seismicity obtained from the Advanced National Seismic System (ANSS) catalog for each day in each box is uniformly spread over that box plus the eight immediately adjacent boxes, known as the Moore neighborhood (Moore 1962). The resulting smoothed intensities for each box is a time series.
3. Only the top 10% most active boxes are considered. These are the boxes with the most $M_c \geq 3.0$ earthquakes during the period t_0 = 1 January 1950 to t_2 = 1 August 2005. M_c is the cutoff, or completeness, magnitude for the analysis.
4. Each time series is normalized in time by subtracting the temporal mean and dividing by the temporal standard deviation.
5. Each time series is then normalized in space for each value of time by subtracting the spatial mean and dividing by the spatial standard deviation.
6. Two intensity maps $I_1(x_i, t_b, t_1)$, $I_2(x_i, t_b, t_2)$ are computed by averaging all the time series from an initial time t_b to t_1 where $t_0 < t_b < t_1$, and then from t_b to t_2. Here t_0 = 1 January 1950, t_1 = 1 January 1985, and t_2 = 1 August 2005.
7. The intensity change $\Delta I(x_i, t_b, t_1, t_2) = I_2(x_i, t_b, t_2) - I_1(x_i, t_b, t_1)$ is computed at each location and absolute value is taken $|\Delta I(x_i, t_b, t_1, t_2)|$.
8. The average of $|\Delta I(x_i, t_b, t_1, t_2)|$ over all values of $t_0 < t_b < t_{max}$ is then computed.
9. Finally, the mean squared change $<|\Delta I(x_i, t_b, t_1, t_2)|>^2$ is computed.

Note that steps (2), (3), (7), and (8) have been modified from the original published algorithm (Rundle *et al.* 2002, 2003; Tiampo *et al.* 2002a, 2000c).

Hot-spot pixels are defined to be the regions where $\Delta P_i(t_0, t_1, t_2)$ is larger than some threshold value in the interval [0, 1]. In these regions, $P_i(t_0, t_1, t_2)$ is larger than the average value for all boxes (the background level). Note that since the intensities are squared in defining probabilities the hot spots may be due to either increases of seismic activity during the change-time interval (activation) or due to decreases (quiescence). We hypothesize that earthquakes with magnitudes larger than $M_c + 2$ will occur preferentially in hot spots during the forecast-time interval t_2 to t_3. Note that this is a binary forecast: An earthquake is either forecast to occur or it is forecast not to occur.

RELATIVE INTENSITY

An alternative approach to earthquake forecasting is to use the rate of occurrence of small earthquakes in the past. We refer to this type of forecast as a relative intensity (RI) forecast. In such a forecast, the study region is again tiled with boxes of size 0.1° by 0.1°. The number of earthquakes with magnitude $M \geq 3.0$ in each box is determined over the time period from t_0 to t_2. The RI score for each box is then computed as the total number of earthquakes in the box in the time period divided by the value for the box having the largest value. In order to create a binary forecast, a threshold value in the interval [0, 1] is selected. Large earthquakes having $M \geq M_c + 2$ are then considered possible only in boxes having an RI value larger than the threshold. The physical justification for this type of forecast is that large earthquakes are considered most likely to occur at sites of high seismic activity. In this paper we combine our binary PI forecast with a continuum RI forecast in order to create our continuum RELM forecast.

BINARY VERSUS CONTINUUM FORECASTS

The earthquake forecast made by the PI method is a binary forecast. An earthquake is forecast to occur in the hot spot regions and not to occur in the other regions, analogous to the issuance of tornado warnings. An extensive methodology has been developed in the atmospheric sciences for forecast verification. A standard approach uses contingency tables and relative operating characteristic (ROC) diagrams (Jolliffe and Stephenson 2003). An example of binary forecast construction and verification is presented in appendix B.

The alternative to binary forecasts is a continuum forecast. The likelihood of an earthquake throughout the entire region is specified, analogous to temperature forecasts in the atmospheric sciences. A common approach to testing the validity of these forecasts is the maximum likelihood test. Kagan and Jackson (2000) were the first to apply this test to earthquake forecasts. The maximum likelihood test is not useful for the verification of some types of earthquake forecasts because it is overly sensitive to the least probable events. For example, consider two forecasts. The first perfectly forecasts 99 out of 100 events but assigns zero probability to the last event. The second assigns zero probability to all 100 events. Under a likelihood test, both forecasts will have the same skill score of zero. Furthermore, a naive forecast that assigns uniform probability to all possible sites will always score higher than a forecast that misses only a single event but is otherwise superior.

CREATING THE FORECAST MAP

The PI method finds regions where earthquakes are most likely to occur during a future time-window. In order to create a forecast map suitable for RELM testing, we combined the PI map with the RI map to create a probability map. This map is then renormalized to unit probability and scaled by the total number of $M \geq 5$ earthquakes expected over the future five-year period. The details of this procedure are as follows:

1. We first created a relative intensity map for the entire region to be considered. Data was taken from the ANSS online catalog for the years 1950 to 2005. This data was then truncated such that relative values greater than 10^{-1} were set to 10^{-1} and nonzero values less than 10^{-4} were set to 10^{-4}. Finally, since the RELM calculations cannot handle zero-rate values, every box with zero historic seismicity

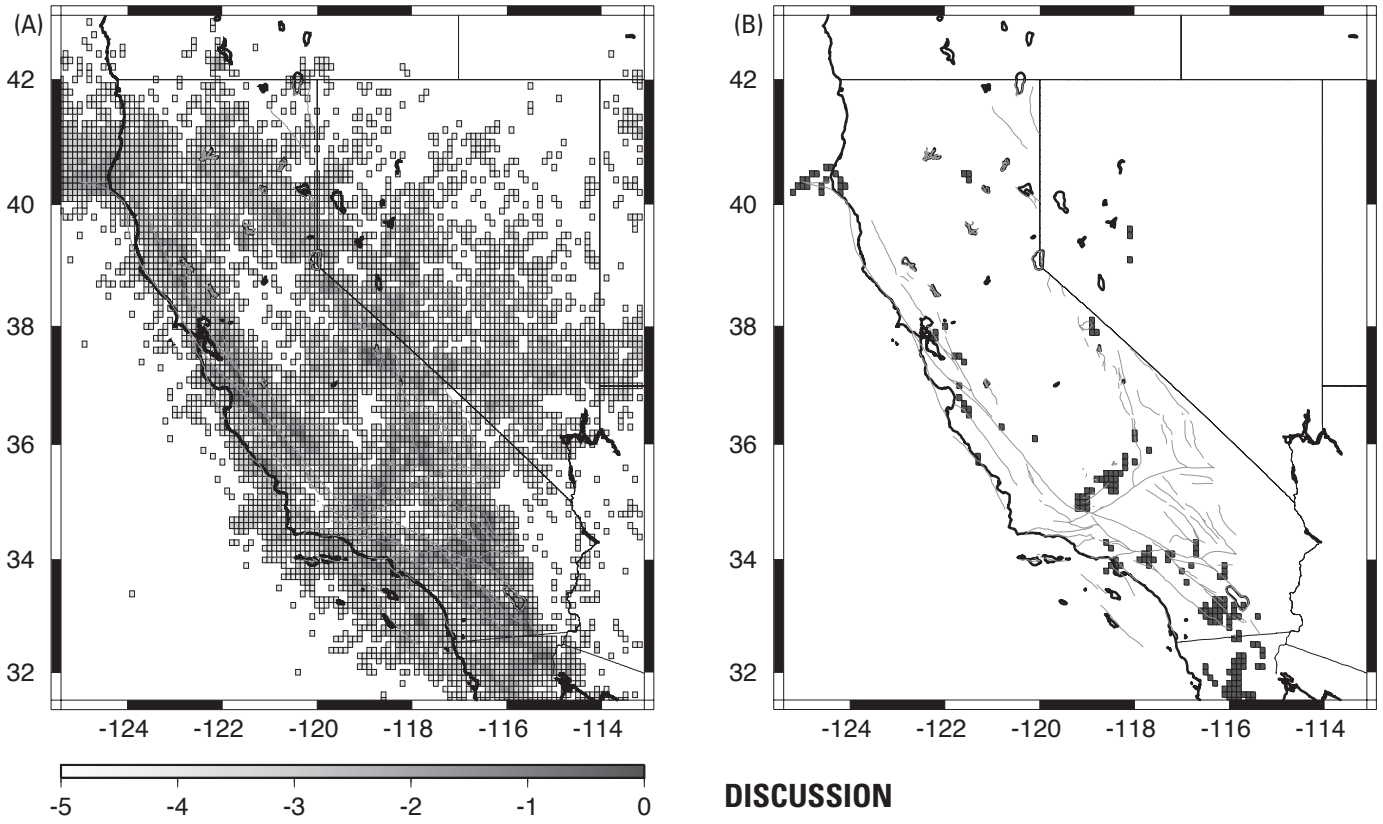

▲ **Figure 1.** (A) Relative intensity (RI) map for all of California and the surrounding region. Data from the ANSS online catalog for the years 1950 to 2005 were used. (B) Pattern informatics (PI) map for the same region and time frame as above.

was given a value of 10^{-5}. The RI map is shown in figure 1(A).

2. We next perform a pattern informatics calculation over the top 10% of most active sites in California using the ANSS catalog as input. For this calculation, we used t_0 = 1 January 1950, t_1 = 1 January 1985, and t_2 = 1 August 2005. Since the hot spots are where we expect future earthquakes to occur, they are given a probability value of unity. The PI map is shown in figure 1(B).
3. We then create a composite probability map by superimposing the PI map and its Moore neighborhood (the pixel plus its eight adjacent neighbors) on top of the RI map. All the hot-spot pixels have a probability of 1, and all other pixels have probabilities that range from 10^{-5} to 10^{-1}. The composite map is shown in figure 2.
4. To convert our pixel probabilities to earthquake occurrence probabilities, we first sum the probabilities in all pixels in the region and call this sum N. We then normalize this total to the expected number of $M \geq 5.0$ earthquakes during the forecast period. We estimate four to eight such events per year and assume 30 such events during a five-year period. In order to do this, we multiply each pixel probability by $30/N$ to give our RELM forecast. We then use Gutenberg-Richter scaling to interpolate these rates into the appropriate magnitude bins specified by the RELM test.

DISCUSSION

Ultimately there exists the fundamental question of whether forecasts of the time and location of future earthquakes can be accurately made. It is accepted that long-term hazard maps of the expected rate of occurrence of earthquakes are reasonably accurate. But is it possible to do better? Are there precursory phenomena that will allow earthquakes to be forecast?

It is actually quite surprising that immediate local precursory phenomena are not seen. Prior to a volcanic eruption, increases in regional seismicity and surface movements are generally observed. For a fault system, the stress gradually increases until it reaches the frictional strength of the fault and a rupture is initiated. It is certainly reasonable to hypothesize that the stress increase would cause increases in background seismicity and aseismic slip. In order to test this hypothesis, the Parkfield Earthquake Prediction Experiment was initiated in 1985. The expected Parkfield earthquake occurred beneath the heavily instrumented region on 28 September 2004. No local precursory changes were observed (Borcherdt *et al.* 2006).

In the absence of local precursory signals, the next question is whether broader anomalies develop, and in particular whether there is anomalous seismic activity. It is this question that is addressed in this paper. Using a technique that has been successfully applied to the forecasting of El Niño, we have developed a systematic pattern informatics approach to the identification of regions of anomalous seismic activity. Applications of

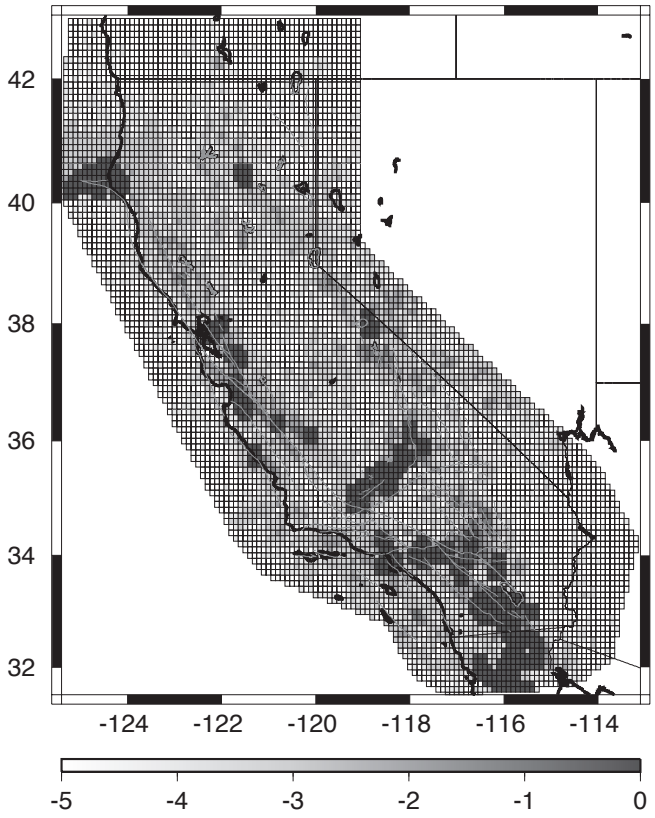

▲ **Figure 2.** Composite forecast map. The scaled PI and RI maps have been combined, and boxes outside the testing region have been discarded.

this technique to California, Japan, and on a worldwide basis have successfully forecast the location of future earthquakes. We emphasize that this is not an earthquake prediction. It is a forecast of where future earthquakes are expected to occur during a future time window of five to 10 years. The objective is to reduce the possible future sites of earthquakes relative to a long-term hazard assessment map.

ACKNOWLEDGMENTS

This work has been supported by NASA Headquarters under the Earth System Science Fellowship Grant NGT5 (JRH), by research support from the National Science Council and the Department of Earth Sciences (CCC), by an HSERC Discovery grant (KFT), by a grant from the U.S. Department of Energy, Office of Basic Energy Sciences to the University of California, Davis DE-FG03-95ER14499 (JRH and JBR), and through additional funding from NSF grant ATM-0327558 (DLT) and the National Aeronautics and Space Administration under grants through the Jet Propulsion Laboratory (AD) to the University of California, Davis.

REFERENCES

Borcherdt, R. D., M. J. S. Johnston, G. Glassmoyer, and C. Dietel (2006). Recordings of the 2004 Parkfield earthquake on the General Earthquake Observation System Array: Implications for earthquake precursors, fault rupture, and coseismic strain changes. *Bulletin of the Seismological Society of America* **96**, 73–89.

Bowman, D. D., G. Ouillon, C. G. Sammis, A. Sornette, and D. Sornette (1998). An observational test of the critical earthquake concept. *Journal of Geophysical Research* **103**, 24,359–24,372.

Holliday, J. R., J. B. Rundle, K. F. Tiampo, W. Klein, and A. Donnellan (2007). Systematic procedural and sensitivity analysis of the pattern informatics method for forecasting large ($M \geq 5$) earthquake events in southern California. *Pure and Applied Geophysics*, forthcoming.

Jolliffe, I. T., and D. B. Stephenson (2003). *Forecast Verification*. Chichester, England and Hoboken, NJ: John Wiley.

Kagan, Y. Y., and D. D. Jackson (2000). Probabilistic forecasting of earthquakes. *Geophysical Journal International* **143**, 438–453.

Kanamori, H. (2003). Earthquake prediction: An overview. In *International Handbook of Earthquake & Engineering Seismology*, ed. W. H. K. Lee, H. Kanamori, P. Jennings, and C. Kisslinger, 1,205–1,216. Amsterdam and Boston: Academic Press.

Kossobokov, V. G., V. I. Keilis-Borok, D. L. Turcotte, and B. D. Malamud (2000). Implications of a statistical physics approach for earthquake hazard assessment and forecasting. *Pure and Applied Geophysics* **157**, 2,323–2,349.

Mason, I. B. (2003). Binary events. In *Forecast Verification*, ed. I. T. Joliffe and D. B. Stephenson, 37–76. Chichester, England and Hoboken, NJ: John Wiley.

Molchan, G. M. (1997). Earthquake predictions as a decision-making problem. *Pure and Applied Geophysics* **149**, 233–247.

Moore, E. F. (1962). Machine models of self reproduction. In *Proceedings of the Fourteenth Symposium on Applied Mathematics*, 17–33. American Mathematical Society.

Rundle, J. B., K. F. Tiampo, W. Klein, and J. S. S. Martins (2002). Self-organization in leaky threshold systems: The influence of near-mean field dynamics and its implications for earthquakes, neurobiology, and forecasting. *Proceedings of the National Academy of Sciences of the United States of America* **99**, 2,514–2,521: Supplement 1.

Rundle, J. B., D. L. Turcotte, R. Shcherbakov, W. Klein, and C. Sammis (2003). Statistical physics approach to understanding the multiscale dynamics of earthquake fault systems. *Reviews of Geophysics* **41** (4), 1,019.

Swets, J. A. (1973). The relative operating characteristic in psychology. *Science* **182**, 990–1,000.

Tiampo, K. F., J. B. Rundle, S. McGinnis, S. J. Gross, and W. Klein (2002a). Eigenpatterns in southern California seismicity. *Journal of Geophysical Research* **107** (B12), 2,354.

Tiampo, K. F., J. B. Rundle, S. McGinnis, S. J. Gross, and W. Klein (2002b). Mean field threshold systems and earthquakes: An application to earthquake fault systems. *Europhysics Letters* **60** (3), 481–487.

Tiampo, K. F., J. B. Rundle, S. McGinnis, and W. Klein (2002c). Pattern dynamics and forecast methods in seismically active regions. *Pure and Applied Geophysics* **159**, 2,429–2,467.

Turcotte, D. L. (1991). Earthquake prediction. *Annual Review of Earth and Planetary Sciences* **19**, 263–281.

Wyss, M., and R. E. Habermann (1988). Precursory seismic quiescence. *Pure and Applied Geophysics* **126**, 319–332.

Center for Computational Science and Engineering
University of California—Davis
One Shields Avenue
Davis, California 95616-8572 USA
holliday@cse.ucdavis.edu
(J.R.H.)

Appendix A—Forecast Verification

Along with the RELM test, previous published tests of earthquake forecasts have emphasized the likelihood test (Kagan and Jackson 2000; Rundle *et al.* 2002; Tiampo *et al.* 2002c; Holliday *et al.* 2005). As discussed above, these tests have the significant disadvantage that they are overly sensitive to the least probable events. For this reason, likelihood tests are subject to unconscious bias.

An extensive review on forecast verification in the atmospheric sciences has been conducted by Jolliffe and Stephenson (2003). The wide varieties of approaches that they consider are directly applicable to earthquake forecasts as well. We believe that many of these approaches are better suited to the evaluation of earthquake forecasts. The earthquake forecasts considered in this paper can be viewed as binary forecasts by considering the events (earthquakes) as being forecast either to occur or not to occur in a given box. We consider that there are four possible outcomes for each box, thus two ways to classify each hot-spot box, and two ways to classify each nonhot-spot box:

1. An event occurs in a hot-spot box or within the Moore neighborhood of the box (the Moore neighborhood consists of the forecast box and its eight surrounding boxes). This is a success.
2. No event occurs in a white nonhot-spot box. This is also a success.
3. No event occurs in a hot-spot box or within the Moore neighborhood of the hot-spot box. This is a false alarm.
4. An event occurs in a white, nonhot-spot box. This is a failure-to-predict.

We note that these rules tend to give credit, as successful forecasts, for events that occur very near hot-spot boxes. We have adopted these rules in part because the grid of boxes is positioned arbitrarily on the seismically active region; thus we allow a margin of error of ±1 box dimension. In addition, the events we are forecasting are large enough so that their source dimensions approach, and can even exceed, the box dimension, meaning that an event might have its epicenter outside a hot-spot box, but the rupture might then propagate into the box. Other similar rules are possible but we have found that all such rules basically lead to similar results.

The standard approach to the evaluation of a binary forecast is the use of a relative operating characteristic (ROC) diagram (Swets 1973; Mason 2003). Standard ROC diagrams consider the fraction of failures-to-predict and the fraction of false alarms. This method evaluates the performance of the forecast method relative to random chance by constructing a plot of the fraction of failures-to-predict against the fraction of false alarms for an ensemble of forecasts. Molchan (1997) has used a modification of this method to evaluate the success of intermediate-term earthquake forecasts.

The binary approach has a long history, more than 100 years, in the verification of tornado forecasts (Mason 2003). These forecasts take the form of a tornado forecast for a specific location and time interval, each forecast having a binary set of possible outcomes. For example, during a given time window of several hours' duration, a forecast is issued in which a list of counties is given with a statement that one or more tornadoes will or will not occur. A 2 × 2 *contingency table* is then constructed. The top row contains the counties in which tornadoes are forecast to occur and the bottom row contains counties in which tornadoes are forecast to not occur. Similarly, the left column represents counties in which tornadoes were actually observed, and the right column represents counties in which no tornadoes were observed.

With respect to earthquakes, our forecasts take exactly this form. A time window is proposed during which the forecast of large earthquakes having a magnitude above some minimum threshold is considered valid. An example might be a forecast of earthquakes larger than $M = 5$ during a period of five or 10 years' duration. A map of the seismically active region is then completely covered ("tiled") with boxes of two types: boxes in which the epicenters of at least one large earthquake are forecast to occur and boxes in which large earthquakes are forecast to not occur. In other types of forecasts, large earthquakes are given some continuous probability of occurrence from 0% to 100% in each box (Kagan and Jackson 2000). These forecasts can be converted to the binary type by the application of a *threshold* value. Boxes having a probability below the threshold are assigned a forecast rating of *nonoccurrence* during the time window, while boxes having a probability above the threshold are assigned a forecast rating of *occurrence*. A high threshold value may lead to many *failures-to-predict* (events that occur where no event is forecast), but few *false alarms* (an event is forecast at a location but no event occurs). The level at which the threshold is set is then a matter of public policy specified by emergency planners, representing a balance between the prevalence of failures-to-predict and false alarms.

Appendix B—Binary Earthquake Forecast Verification

To illustrate this approach to earthquake forecast verification, we have constructed two types of retrospective binary forecasts for California. The first type of forecast utilizes the PI results published by Rundle *et al.* (2002) and Tiampo *et al.* (2002c) for southern California and adjacent regions (32° to 38.3° N lat, 238° to 245° E long). This forecast was constructed for the time period 1 January 2000 to 31 December 2009, but we performed an interim analysis using data up to 30 June 2005. The second type of forecast utilizes the RI results with the same parameter thresholds.

The first step in our generation of ROC diagrams is the construction of the 2 × 2 contingency table for the PI and RI forecast maps. The hot-spot boxes in each map represent the forecast locations. A hot-spot box upon which *at least* one large future earthquake during the forecast period occurs is counted as a *successful forecast*. A hot-spot box upon which *no* large future earthquake occurs during the forecast period is counted as an *unsuccessful forecast*, or alternately, a *false alarm*. A white box upon which *at least* one large future earthquake during the forecast period occurs is counted as a *failure-to-predict*. A white box

upon which *no* large future earthquake occurs during the forecast period is counted as an *unsuccessful forecast of nonoccurrence*.

Verification of the PI and RI forecasts proceeds in exactly the same way as for tornado forecasts. For a given number of hot-spot boxes, which is controlled by the value of the probability threshold in each map, the contingency table (see table B.1) is constructed for both the PI and RI maps. Values for the table elements a (forecast = yes, observed = yes), b (forecast = yes, observed = no), c (forecast = no, observed = yes), and d (forecast = no, observed = no) are obtained for each map. The fraction of colored boxes, also called the *probability of forecast of occurrence*, is $r = (a + b) / N$, where the total number of boxes is $N = a + b + c + d$. The *hit rate* is $H = a / (a + c)$ and is the fraction of large earthquakes that occur on a hot spot. The *false alarm rate* is $F = b / (b + d)$ and is the fraction of nonobserved earthquakes that are incorrectly forecast.

To analyze the information in the PI and RI maps, the standard procedure is to consider all possible forecasts together. These are obtained by increasing F from 0 (corresponding to no hot spots on the map) to 1 (all active boxes on the map are identified as hot spots). The plot of H versus F is the ROC diagram. Varying the threshold value for both the PI and RI forecasts, we have obtained the values of H and F given in figure B.1. The results corresponding to the contingency tables given in tables B.1 and B.2 are given by the filled symbols. The forecast with 29 hot-spot boxes has $F_{PI} = 0.00498$, $H_{PI} = 0.235$ and $F_{RI} = 0.00537$, $H_{RI} = 0.125$. The forecast with 127 hot-spot boxes has $F_{PI} = 0.0207$, $H_{PI} = 0.719$ and $F_{RI} = 0.0213$, $H_{RI} = 0.666$. Also shown in figure B.1 is a gain curve defined by the ratio of $H_{PI}(F)$ to $H_{RI}(F)$. Gain values greater than unity indicate better performance using the PI map than using the RI map. The horizontal dashed line corresponds to zero gain. From figure B.1 it can be seen that the PI approach outperforms (is above) the RI under many circumstances, and both outperform a random map, where $H = F$, by a large margin. For reference, ROC diagrams using the modified method discussed in the main text for the same forecast period are given in figure B.2. Note that a different input catalog was used for this analysis. Also note that in this case, the PI approach outperforms the RI under all circumstances.

TABLE B.1
Contingency tables as a function of false alarm rate. Threshold value chosen such that $F \approx 0.005$.

	Pattern informatics (PI) forecast				Relative intensity (RI) forecast		
	Observed				Observed		
Forecast	Yes	No	Total	Forecast	Yes	No	Total
Yes	(a) 4	(b) 25	29	Yes	(a) 2	(b) 27	29
No	(c) 13	(d) 4998	5011	No	(c) 14	(d) 4997	5011
Total	17	5023	5040	Total	16	5024	5040

TABLE B.2
Contingency tables as a function of false alarm rate. Threshold value chosen such that $F \approx 0.021$.

	Pattern informatics (PI) forecast				Relative intensity (RI) forecast		
	Observed				Observed		
Forecast	Yes	No	Total	Forecast	Yes	No	Total
Yes	(a) 23	(b) 104	127	Yes	(a) 20	(b) 107	127
No	(c) 9	(d) 4904	4913	No	(c) 10	(d) 4903	4913
Total	32	5008	5040	Total	30	5010	5040

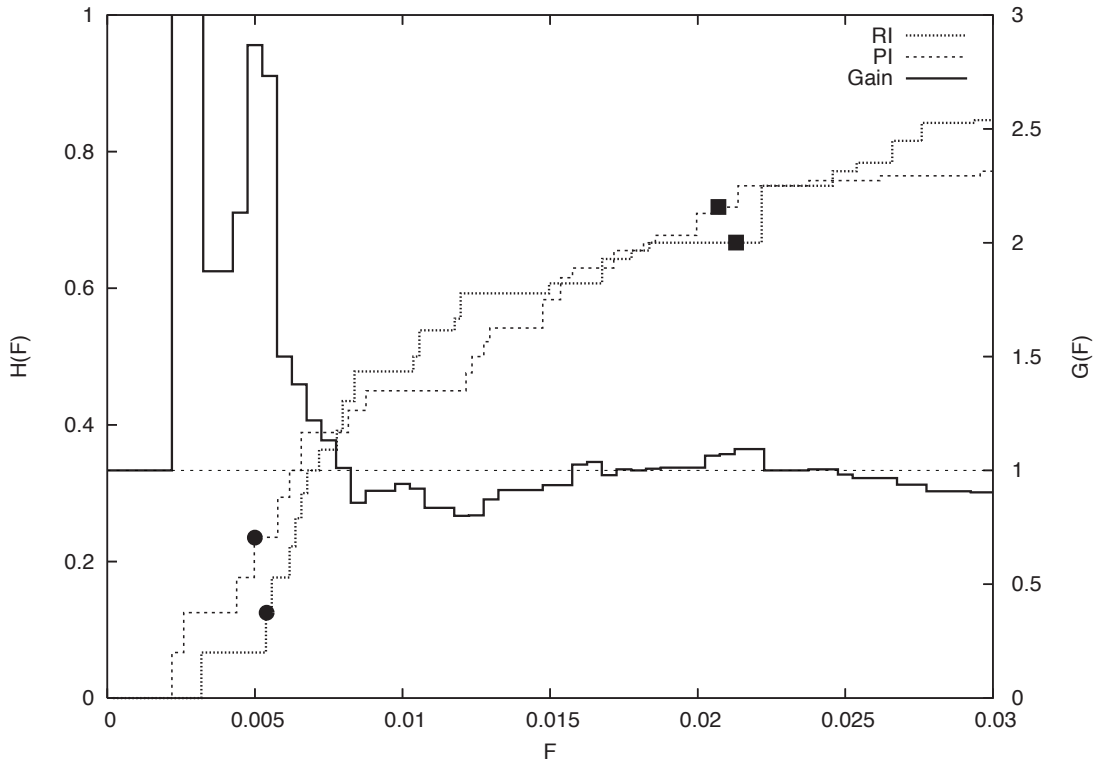

▲ **Figure B.1.** Relative operating characteristic (ROC) diagram. Plot of hit rates, H, versus false alarm rates, F, for the PI forecast and RI forecast. Also shown is the gain ratio defined as $H_{PI}(F) / H_{RI}(F)$. The filled symbols correspond to the threshold values used in tables B.1 and B.2, solid circles for 29 hot-spot boxes and solid squares for 127 hot-spot boxes. The horizontal dashed line corresponds to zero gain.

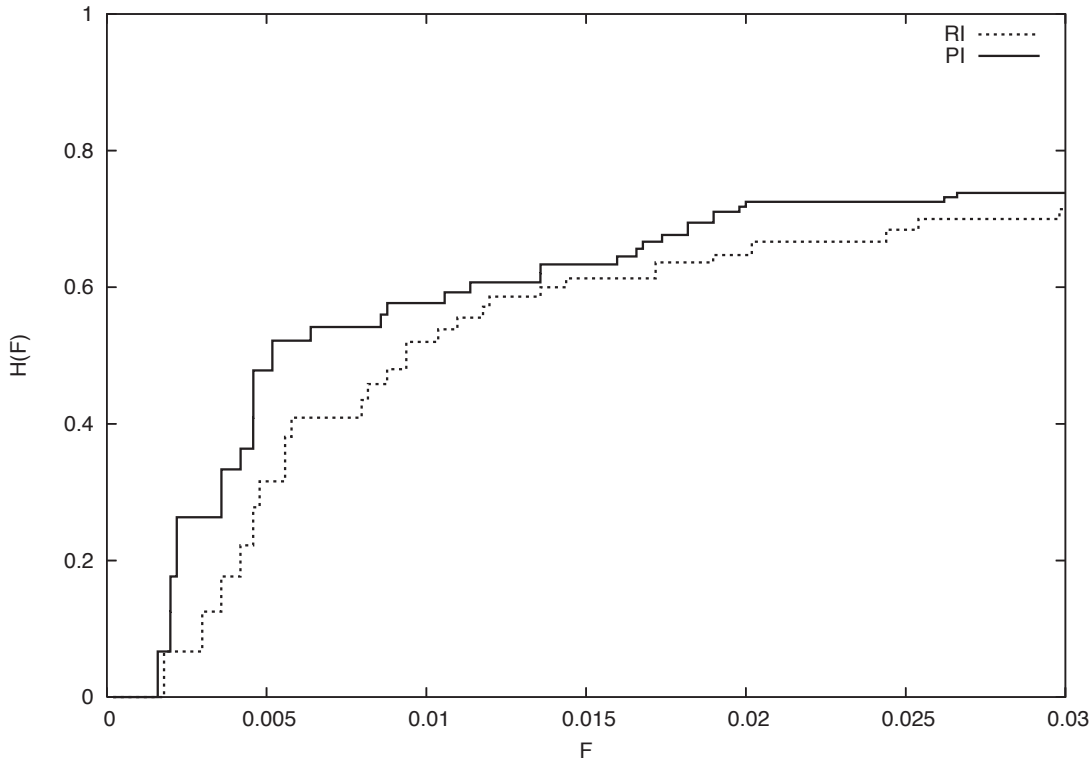

▲ **Figure B.2.** Relative operating characteristic (ROC) diagram. Plot of hit rates, H, versus false alarm rates, F, for the RI forecast and PI forecast using the modified method. Note that the PI approach outperforms the RI under all circumstances.